Author's personal copy

Precision Agric (2012) 13:473–500
DOI 10.1007/s11119-012-9263-8

Mapping radiation interception in row-structured orchards using 3D simulation and high-resolution airborne imagery acquired from a UAV

M. L. Guillen-Climent · Pablo J. Zarco-Tejada · J. A. J. Berni · P. R. J. North · F. J. Villalobos

Published online: 20 March 2012
© Springer Science+Business Media, LLC 2012

Abstract This study was conducted to model the fraction of intercepted photosynthetically active radiation (fIPAR) in heterogeneous row-structured orchards, and to develop methodologies for accurate mapping of the instantaneous fIPAR at field scale using remote sensing imagery. The generation of high-resolution maps delineating the spatial variation of the radiation interception is critical for precision agriculture purposes such as adjusting management actions and harvesting in homogeneous within-field areas. *Scaling-up* and model inversion methods were investigated to estimate fIPAR using the 3D radiative transfer model, Forest Light Interaction Model (FLIGHT). The model was tested against airborne and field measurements of canopy reflectance and fIPAR acquired on two commercial peach and citrus orchards, where study plots showing a gradient in the canopy structure were selected. High-resolution airborne multi-spectral imagery was acquired at 10 nm bandwidth and 150 mm spatial resolution using a miniaturized multi-spectral camera on board an unmanned aerial vehicle (UAV). In addition, simulations of the land surface bidirectional reflectance were conducted to understand the relationships between canopy architecture and fIPAR. Input parameters used for the canopy model, such as the leaf and soil optical properties, canopy architecture, and sun geometry were studied in order to assess the effect of these inputs on canopy reflectance, vegetation indices and fIPAR. The 3D canopy model approach used to simulate the discontinuous row-tree canopies yielded spectral RMSE values below 0.03 (visible region) and below 0.05 (near-infrared) when compared against airborne canopy reflectance imagery acquired over the

M. L. Guillen-Climent · P. J. Zarco-Tejada (✉) · J. A. J. Berni · F. J. Villalobos
Instituto de Agricultura Sostenible (IAS), Consejo Superior de Investigaciones Científicas (CSIC), Alameda del Obispo, s/n, 14004 Córdoba, Spain
e-mail: pzarco@ias.csic.es
URL: http://quantalab.ias.csic.es

P. R. J. North
Environmental Modelling and Earth Observation Group, Department of Geography, University of Wales, Swansea SA2 8PP, UK

F. J. Villalobos
Departamento de Agronomía, Universidad de Córdoba, Campus Universitario de Rabanales, 14014 Córdoba, Spain

Author's personal copy

sites under study. The FLIGHT model assessment conducted for fIPAR estimation against field measurements yielded RMSE values below 0.08. The simulations conducted suggested the usefulness of these modeling methods in heterogeneous row-structured orchards, and the high sensitivity of the normalized difference vegetation index and fIPAR to background, row orientation, percentage cover and sun geometry. Mapping fIPAR from high-resolution airborne imagery through *scaling-up* and model inversion methods conducted with the 3D model yielded RMSE error values below 0.09 for the *scaling-up* approach, and below 0.10 for the model inversion conducted with a look-up table. The generation of intercepted radiation maps in row-structured tree orchards is demonstrated to be feasible using a miniaturized multi-spectral camera on board UAV platforms for precision agriculture purposes.

Keywords Remote sensing · fIPAR · NDVI · Airborne imagery · UAV · Row-structured tree canopies · Radiative transfer model · *Scaling-up* · Model inversion

Introduction

Intercepted photosynthetically active radiation (IPAR) by a crop canopy is the main factor determining dry matter production under non-limiting water and nutrients supply conditions (Gallagher and Biscoe 1978; Hunt 1994). The influence of radiation levels on crop photosynthesis and biomass accumulation was proposed in the late 1950s by work developed by De Wit (1959) and Loomis and Williams (1963), which showed a close link between the amount of radiation received by a crop and its growth. It was Monteith (1972) who first distinguished the crop function in absorbing and transforming the intercepted solar energy into biomass. Further studies investigated the relationships between the incident solar radiation and the limiting factors determining the light interception in crop canopies, showing that leaf area index (LAI) is the dominant factor in the case of continuous canopies (e.g., Lang et al. 1985). Fruit tree orchards, however, are grown as discontinuous canopies, and the amount of PAR intercepted depends primarily on the orchard architecture, which varies with planting system, tree spacing, tree shape, tree height, alley width, row orientation as well as LAI (Jackson 1980; Robinson and Lakso 1991). Examining within-field variability to optimize crop yield and production has been a target of precision agriculture in the early 1980s. In this context, maps of fraction of intercepted photosynthetically active radiation (fIPAR) variability, crop yield or crop nutrient, derived from image-based remote sensing techniques, have been presented as potential benefits for precision crop management (Moran et al. 1997).

Several previous studies investigated the feasibility of estimating the fraction of photosynthetically active radiation intercepted (fIPAR) and absorbed (fAPAR) using methods based on optical remote sensing. Measurements of IPAR and/or the related fraction of intercepted PAR (fIPAR) can be time consuming because of the need to sample for spatial and temporal variability. In this context, remote sensing techniques are useful enabling the assessment of large areas. Spectral vegetation indices (SVI) based on contrasting canopy reflectance in the red and near-infrared (NIR) bands were applied to assess fIPAR and fAPAR at canopy-level scales, finding that the normalized difference vegetation index (NDVI) was the best correlated (Asrar et al. 1992; North 2002). Empirical and modeled relationships between SVI and fIPAR were obtained in homogeneous canopies, such as wheat, maize or soybean crops (e.g., Daughtry et al. 1983; Hall et al. 1992; Moriondo et al. 2007) and forest canopies (e.g., Myneni and Williams 1994; Huemmrich 2001; Zhang et al.

Author's personal copy

2009). Later, the sensitivity of these relationships between SVI and the fraction of PAR, absorbed or intercepted, was investigated using 3D models of radiative transfer in plant canopies. Work developed by Huete (1989), Choudhury (1987) and Huemmrich and Goward (1997) showed the sensitivity of these relationships with the canopy architecture, the optical properties of the canopy elements and the background. However, these studies were focused on randomly distributed canopy elements and closed canopy forestry areas. Only a limited number of studies have focused on heterogeneous canopies such as the row-structured open-tree canopies, therefore the application of such random-distribution scenarios on these relationships may not be valid. The effects due to the row orientation, soil background and the viewing geometry on remote sensing vegetation indices and canopy reflectance used to estimate instantaneous fIPAR need appropriate modeling strategies. In particular, radiative transfer models that aim at deriving the amount and distribution of fIPAR by the crop canopy were reviewed by Mariscal et al. (2000) who developed a model to simulate fIPAR in non-homogeneous olive canopies. Later, the 3D Forest Light Interaction Model (FLIGHT) (North 1996) was used to estimate fAPAR in forest canopies (North 2002; Prieto-Blanco et al. 2009), and model simulations showed the need for accounting for the row structure in orchard canopies (Kempeneers et al. 2008). While methods for modeling and estimating fIPAR in homogenous vegetation are relatively mature, further research is needed for a robust estimate of fIPAR in open canopies, in particular where the architecture of oriented row planting violates the common modeling assumption of angular invariance with respect to solar azimuth. In this research work, a dedicated remote sensing study aiming at assessing the estimation of radiation interception from high-resolution imagery was conducted using an unmanned aerial vehicle (UAV). The quality of remotely sensed fIPAR and fAPAR products requires ensuring a proper verification of the physically-based radiative transfer models that contribute to the retrieval of algorithms used to estimate these products (Pinty et al. 2002). Therefore, 3D radiative transfer models that allow the simulation of local radiation measurements in complex canopy architectures under realistic illumination and sampling conditions are needed (Widlowski 2010). Thus, the objectives of this study were: (i) to use remote sensing data coupled with 3D modeling approaches (forward and inverse) to estimate fIPAR in heterogeneous row-tree canopies using visible (VIS) and NIR bands acquired from a miniaturized multi-spectral camera on board a UAV platform in the context of precision agriculture; and (ii) to assess the effects of the sun angle, row orientation, canopy architecture and background on the canopy reflectance and NDVI used to estimate fIPAR in discontinuous row-tree crop canopies.

Materials and methods

Study area description and field data collection

The ground truth data and airborne imagery required for this study were acquired in 2007 and 2008 in a commercial peach (90-ha) and a citrus (80-ha) orchard located in southern Spain, Cordoba (37°48′N, 4°48′W) and Seville (37°20′N, 5°50′W), respectively. The area has a Mediterranean climate with approximately 600 mm average annual rainfall, mostly concentrated in the autumn–spring period.

The study in the *Prunus persica* (L.) Batsch orchard was conducted in nectarine (cv. Sweet Lady) and peach (cv. Babygold 8) plantations. The nectarine and peach trees were planted in 1990 at 6 m × 3.3 m (500 tree ha^{-1}) and in 1993 at 5 m × 3.3 m (600

Author's personal copy

tree ha^{-1}), respectively, on a deep alluvial soil of loam to clay-loam texture, with rows oriented in the N–S direction. Eight plots were selected from the peach orchard with trees covering a range of LAI from 2 to 4.2, tree height between 2.2 and 4 m, and horizontal crown diameters of 1.4–3.5 m. The study in the citrus orchard was conducted in sweet-orange (*Citrus sinensis* L. Osb cv. Navelina) and clementine-mandarin (*C. clementina* Hort. ex Tan. Cv. Orornules) plantations. The orange and mandarin trees were planted in 1997 at 7 m × 3 m (476 tree ha^{-1}) on a sandy-loam, with rows in E–W direction. Sixteen plots were selected with a range of LAI from 1 to 4, tree height between 1.5 and 4 m, and horizontal crown diameters ranging from 0.8 to 4.5 m. The field campaign was carried out in summer months. Peach trees were fully dressed and had fruits. Orange trees were also fully dressed, as they are perennials, not having fruits at that period. None of them had flowers. In peach orchards, and in general in deciduous fruit orchards, the irrigation season coincides when the trees are fully dressed. Therefore, from an agronomic point of view, the determination of IPAR is critical at this period. The terms intercepted PAR and absorbed PAR are often used interchangeably in the literature; the intercepted PAR (IPAR) is understood as the difference in the PAR flux density above (I_o) and below the plant canopy (the transmittance, T_c). The difference between absorbed PAR and intercepted PAR is $R_s - R_c$, where R_s is the PAR flux density reflected by soil, and R_c the PAR flux density reflected by the canopy.

$$fIPAR = \frac{I_0 - T_c}{I_0} \tag{1}$$

$$fAPAR = \frac{(I_0 + R_s) - (T_c + R_c)}{I_0} \tag{2}$$

This difference is very small for full green canopies (Daughtry et al. 1992). In this study, IPAR and fIPAR were used. Ground measurements were conducted on these selected plots concurrent with the airborne over-flights. The interception of solar radiation by the orchard canopies at each time of day was estimated with a ceptometer (SunScan Canopy Analysis System, Delta-T Devices Ltd, Cambridge, UK). The instrument is composed of two units: (i) a probe, portable instrument 1-m long, for measuring the transmitted photosynthetically active radiation (PAR) flux beneath the canopy; and (ii) a beam fraction sensor (BFS) that measures PAR incident on the canopy at the same time. The BFS incorporates two photodiodes, one of which can be shaded from direct solar radiation by the shade ring. This allows the direct and diffuse components of PAR to be separated. As expected, the fraction of intercepted PAR by a tree is influenced by the rest of the surrounding trees and background. In addition, the crowns are highly overlapped in row-structured tree crops. Therefore, the area comprising the four central trees of each study area was selected to conduct the field measurements of fIPAR. Figure 1a shows imagery acquired by the multispectral airborne sensor at 150 mm spatial resolution, representing two fields used in this study with extreme row orientation angles, and the block of four-trees selected on each study site for field data collection of radiation interception. The high spatial resolution acquired enabled targeting pure scene components, such as pure soil and vegetation, separately as well as on aggregated pixels. The image reflectance extracted for a pure crown, bare soil and aggregated pixels are shown in Fig. 1b. The measurements of transmitted PAR made within the area beneath the four central trees of each plot were in a 1 m × 0.25 m grid, concurrent with the airborne over-flights (Fig. 2). For the assessment of the spatial variation of fIPAR among the different selected plots with a gradient in structural parameters, measurements were conducted at 10.00 GMT (±half-hour). In

Author's personal copy

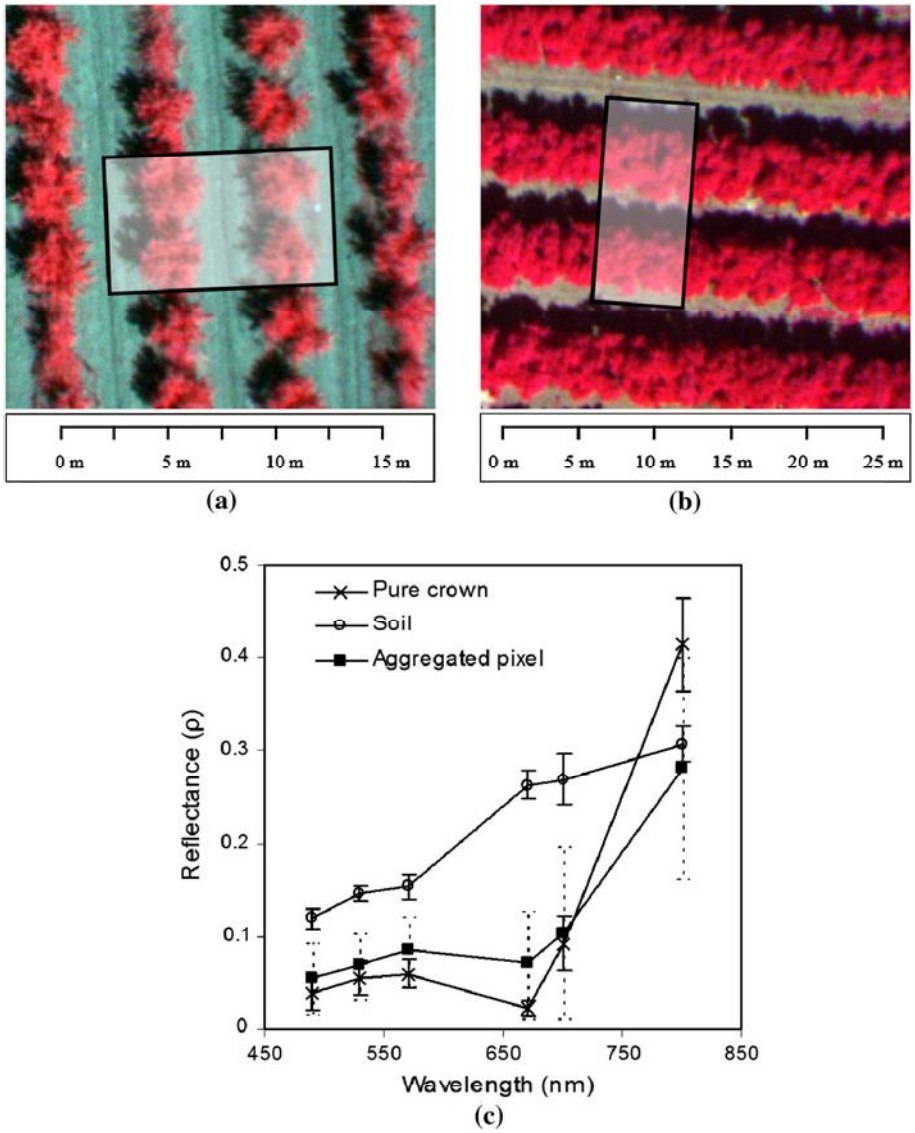

Fig. 1 Multi-spectral reflectance image acquired at 10 nm FWHM and 150 mm spatial resolution acquired from the UAV platform, showing the two fields used in the study, peach (**a**) and citrus (**b**). Canopy reflectance obtained from pure crowns and pure soil pixels, and by aggregating tree crowns, shadows and soil background (**c**)

addition, transmitted and incident PAR measurements were repeated every hour from dawn to noon in one plot per orchard, to assess the diurnal variation of interception solar radiation. The study area where the PAR measurements were conducted and the diurnal variation of interception solar radiation are shown in Fig. 3. The airborne image in this figure shows the bands B: 530 nm, G: 800 nm and R: 670 nm.

Author's personal copy

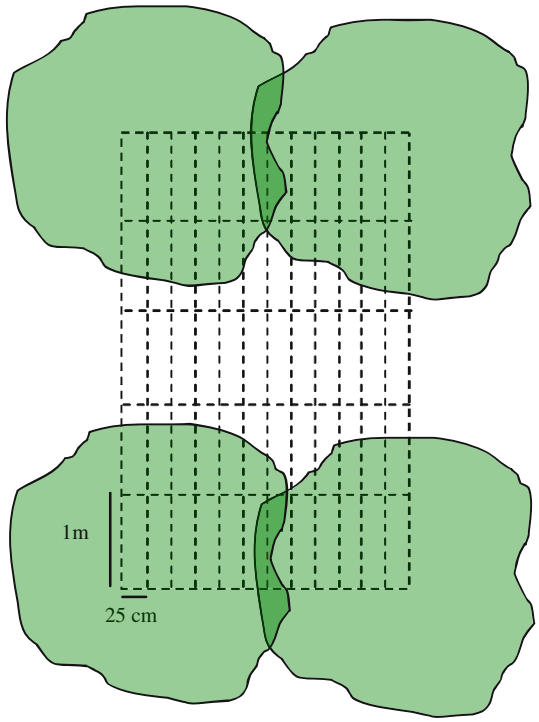

Fig. 2 Schematic view of the grid (1 m × 0.25 m) used for field measurements made by the ceptometer between the four trees per plot (the instrument was orientated in such a way that user's shadow did not affect the measurements)

Parameters used as input for the FLIGHT model were measured in the field at each study plot. Table 1 shows the input parameters required by the model. Single leaf reflectance and transmittance measurements were acquired on leaf samples using an Integrating Sphere (Li-Cor 1800-12, Inc., Lincoln, NE, USA), coupled with a 200-μm diameter single mode fibre to a spectrometer (Ocean Optics Inc. model USB2000, Dunedin, FL, USA). The single leaf values for reflectance (ρ) and transmittance (τ) were acquired as described in the manual of the Li-Cor 1800-12 system (Li-Cor Inc. 1984) and in Zarco-Tejada et al. (2005). More than 150 leaves of peach and orange trees were measured to characterize the leaf optical properties of each crop. Sunlit soil reflectance was extracted from the airborne imagery at the time of each flight. Figure 4 shows the mean leaf reflectance and transmittance measured on peach and orange leaves and used as input for the 3D canopy modeling conducted.

LAI was estimated from the equation (Lang 1987):

$$LAI = -\frac{\cos(\theta) LnT(\theta)}{G(\theta)} \tag{3}$$

where $G(\theta)$, named the G-function, is the mean projection of unit leaf area on a plane normal to the beam; $T(\theta)$ is the transmittance sunbeam, and θ is the solar zenith angle. Taking transmittance measurements with the ceptometer at the time where $\theta = 1$-radian (57.3°), where G-function is close to 0.5 (Ross 1981) the equation yields:

$$LAI = -1.1 LnT(1) \tag{4}$$

The leaf angle distribution function for adult peach and orange trees was calculated according to Lemeur (1973). Random leaf azimuth was assumed. The leaf angle range

Author's personal copy

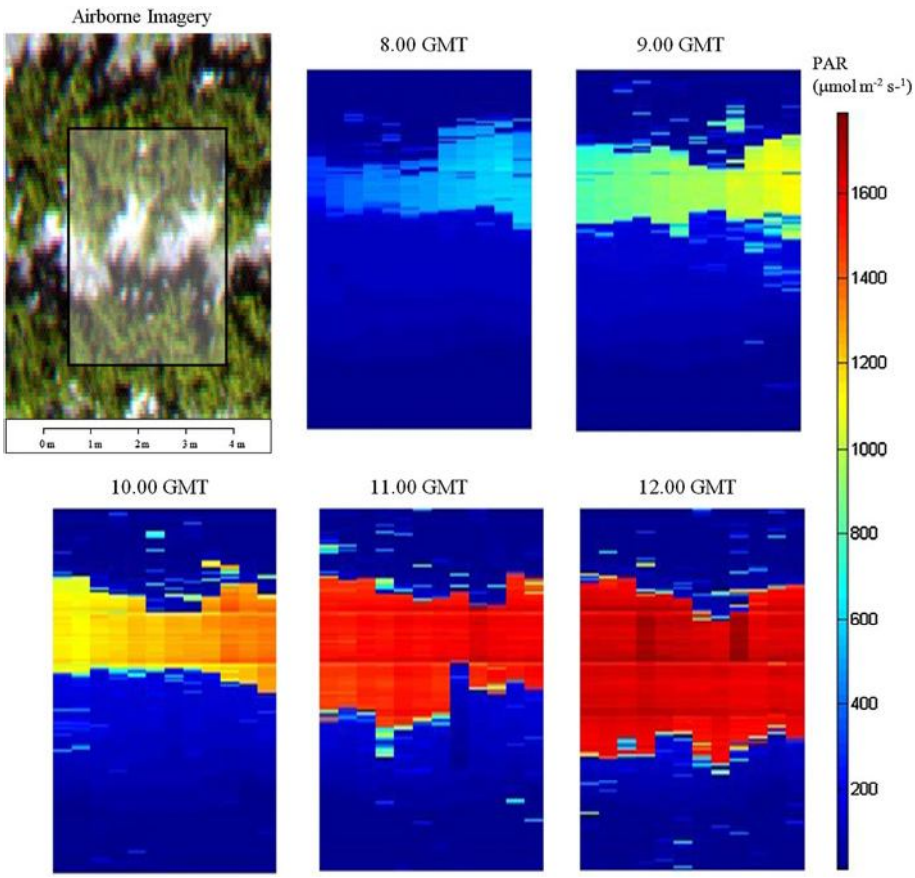

Fig. 3 Airborne imagery acquired from the UAV platform showing one of the study sites (orange orchard, 2007, 14th August, the three bands are: B: 530 nm G: 800 nm R: 670 nm) and diurnal variation of PAR measured by ceptometer at soil level (area shown is the same as in Fig. 2)

(0°–90°) was split into nine intervals of 10° each. The leaf angle density functions $f(\alpha)$, and the corresponding cumulative distribution functions, $F(\alpha)$, were obtained as the relative frequency of leaves with angle α in each α interval (Fig. 5). The leaf inclination was measured in the field with an inclinometer (Fisco Solatronic Inclinometer, Essex, UK), as the angle between the vertical and the normal vector to the upper leaf surface. For each crop, the number of measured leaves of peach and orange was 4 000.

The crown radius and shape, and the height of the fruit trees were measured using a scale pole. The architectural properties for the four central trees of each plot were measured. The trees were divided into its eight octants for measuring horizontal radii and shape (Fig. 6a). In each octant, the tree silhouette was estimated by measuring the upper and the lower limits of the tree-crown with a vertical pole, which was systematically moved away from the tree-trunk in 0.2 m increments (Villalobos et al. 1995) as is shown in Fig. 6b. Table 2 shows the mean values measured for each study plot. Table 2, and Figs. 4 and 5 show the field measurements collected on each study site. These data are later used for the 3D canopy modeling assessment of aggregated reflectance and fIPAR estimation.

Author's personal copy

Table 1 Nominal values and range of parameters used for canopy modelling conducted with FLIGHT for the orchard study sites

FLIGHT input parameters	Description
Leaf optical and structural parameters	
Hemispherical reflectance and transmittance of green leaves	Integrating sphere
Hemispherical reflectance and transmittance of senescent leaves	Not used
Leaf equivalent radius	0.025 m
Canopy layer and structural parameters	
LAI of vegetation	m^2/m^2
Fractional cover	4–70 %
Leaf angle distribution function	9 parameters
Fraction green leaves	1
Fraction senescent leaves	0
Fraction of bark	0
Hemispherical reflectance and transmittance of bark	Not used
Number of stands and position co-ordinates	Co-ordinates (m)
Crown shape	Elliptical
Crown height and radius	m
Trunk height and radius	m
Background and viewing geometry	
Solar zenith and azimuth angles	Degrees
Sensor zenith and azimuth angles	Degrees
Incident PAR	Measured by BFS
Soil reflectance	Image extracted
Soil roughness	0
AOD	0.15

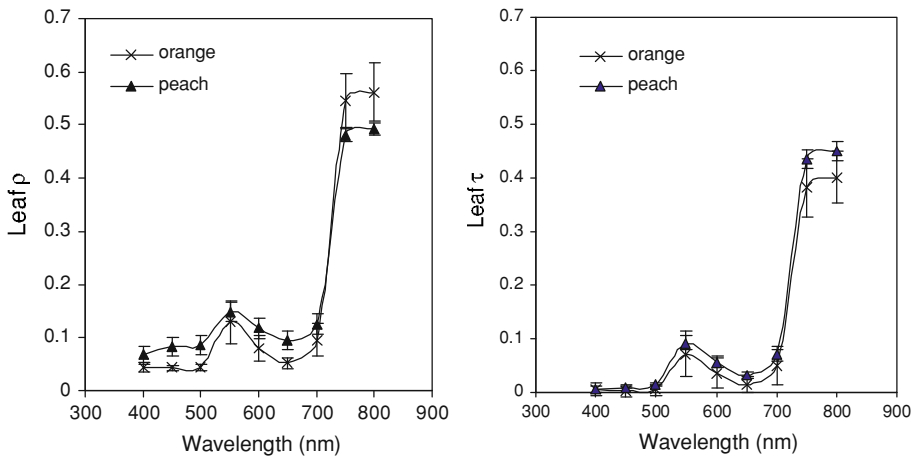

Fig. 4 Reflectance and transmittance measured by integrating sphere for orange and peach leaves

Author's personal copy

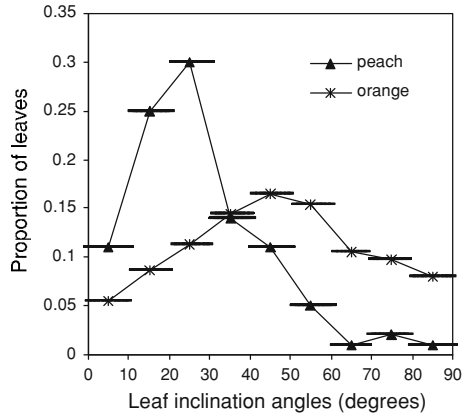

Fig. 5 Leaf angle distribution function in 10° intervals measured for peach and orange trees

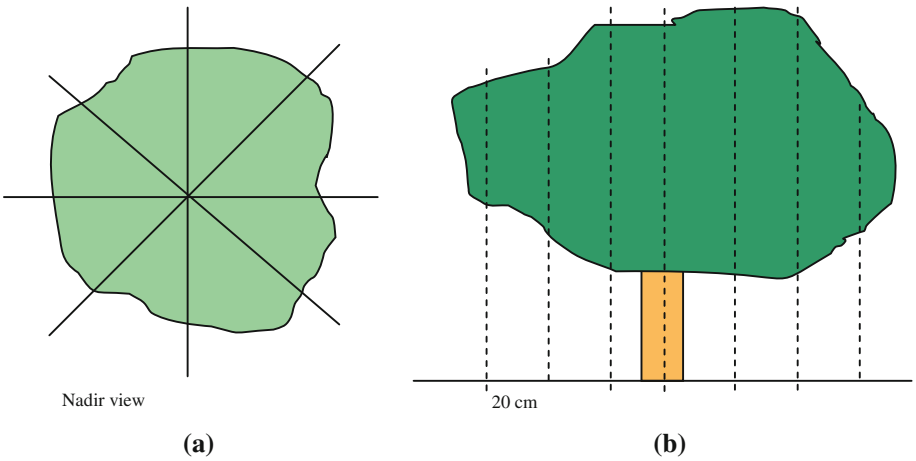

Fig. 6 Schematic view of the **a** nadir and **b** profile view used to measure tree silhouette

Airborne campaigns

The sensor used in this study was a 6-band multi-spectral camera (MCA-6, Tetracam Inc., California, USA) used for biophysical parameter estimation over crops (Berni et al. 2009) and stress detection studies using chlorophyll and PRI bands (Suárez et al. 2009, 2010). An UAV platform for remote sensing research carried the camera (details about the UAV operation can be found in Berni et al. 2009; Zarco-Tejada et al. 2008; Zarco-Tejada et al. 2012). The UAV platform operated in this experiment consisted of a 2-m fixed-wing platform capable of carrying a 3.5 kg payload for 1 h endurance at 5.8 kg take-off weight (TOW) (mX SIGHT, UAV Services and Systems, Germany). The UAV was controlled by an autopilot (AP04, UAV Navigation, Madrid, Spain) for autonomous flight to follow a flight plan using waypoints. The camera consisted of six independent image sensors and optics with user-configurable spectral filters. The image resolution was 1 280 × 1 024 pixels with 10-bit radiometric resolution and optical focal length of 8.5 mm, yielding an angular field of view (FOV) of 42.8°×34.7° and 150-mm pixel spatial resolution at 150-m

Author's personal copy

Table 2 Main characteristics of peach and citrus orchard used for FLIGHT model validation: 14th August 2007 (peach), 16th September 2008 (citrus)

Plot	Time (GMT) and solar angles at image acquisition (SZ°–SA°)		Row orientation	Planting grid (m × m)	Rx (m)	Ry (m)	Tree height (m)
Peach orchard (latitude 37°49′N; longitude 4°53′W)							
1	8.00	62.27°–87.36°	20° NW–SE	5 × 3.3	1.8	1.7	4
1	9.00	50.59°–77.06°	20° NW–SE	5 × 3.3	1.8	1.7	4
1	10.00	35.02°–69.5°	20° NW–SE	5 × 3.3	1.8	1.7	4
1	11.00	29.73°–44.51°	20° NW–SE	5 × 3.3	1.8	1.7	4
2	10.00	35.02°–69.5°	20° NW–SE	5 × 3.3	1.6	1.4	3.6
2	12.00	23.78°–14.68°	20° NW–SE	5 × 3.3	1.6	1.4	3.6
3	10.00	35.02°–69.5°	20° NW–SE	5 × 3.3	0.8	0.6	2.2
3	12.00	23.78°–14.68°	20° NW–SE	5 × 3.3	0.8	0.6	2.2
4	10.00	35.02°–69.5°	20° NW–SE	5 × 3.3	0.9	0.6	2.4
4	12.00	23.78°–14.68°	20° NW–SE	5 × 3.3	0.9	0.6	2.4
5	10.00	35.02°–69.5°	20° NW–SE	5 × 3.3	0.85	0.7	2.3
5	12.00	23.78°–14.68°	20° NW–SE	5 × 3.3	0.85	0.7	2.2
6	10.00	35.02°–69.5°	20° NW–SE	6 × 3.3	1.6	1.5	3.8
6	12.00	23.78°–14.68°	20° NW–SE	6 × 3.3	1.6	1.5	3.8
7	10.00	35.02°–69.5°	20° NW–SE	6 × 3.3	1.4	1.2	3
8	10.00	35.02°–69.5°	20° NW–SE	6 × 3.3	1.4	1.2	3
Orange orchard (latitude 37°20′N; longitude 5°48′W)							
1	8.00	68.11°–76.39°	70° NE–SW	7 × 3	1.75	2.3	4
1	9.00	56.85°–65.21°	70° NE–SW	7 × 3	1.75	2.3	4
1	10.00	47°–49.2°	70° NE–SW	7 × 3	1.75	2.3	4
1	11.00	38.74°–32.31°	70° NE–SW	7 × 3	1.75	2.3	4
1	12.00	34.58°–8.05°	70° NE–SW	7 × 3	1.75	2.3	4
2	10.00	47°–49.2°	70° NE–SW	7 × 3	1.33	1.56	2.48
3	10.00	47°–49.2°	70° NE–SW	7 × 3	1.6	2.45	3.15
4	10.00	47°–49.2°	70° NE–SW	7 × 3	1.8	2.7	4
5	10.00	47°–49.2°	70° NE–SW	7 × 3	1.5	2.05	2.3
6	10.00	47°–49.2°	70° NE–SW	7 × 3	1.15	1.31	2.04
7	10.00	47°–49.2°	70° NE–SW	7 × 3	2	2.3	3.5
8	10.00	47°–49.2°	70° NE–SW	7 × 3	0.4	0.4	1.5
9	10.00	47°–49.2°	70° NE–SW	7 × 3	1.42	2.2	3.2
10	10.00	47°–49.2	70° NE–SW	7 × 3	1	0.9	1.8
11	10.00	47°–49.2°	70° NE–SW	7 × 3	1.5	1.5	2.56
12	10.00	47°–49.2°	70° NE–SW	7 × 3	1.26	2.1	3
13	10.00	47°–49.2°	70° NE–SW	7 × 3	1.6	1.6	2
14	10.00	47°–49.2°	70° NE–SW	7 × 3	1.8	1.6	2.6
15	10.00	47°–49.2°	70° NE–SW	7 × 3	1.8	1.8	3.4
16	10.00	47°–49.2°	70° NE–SW	7 × 3	2	1.7	3.8

Rx crown radius in the row direction, *Ry* crown radius between rows, *SZ* solar zenith (degrees from the vertical), *SA* solar azimuth (degrees from South, clockwise negative)

Author's personal copy

flight altitude. High-resolution multi-spectral images acquired over the peach and citrus orchards enabled the identification of each study site used for field measurements of crop structure and fIPAR. The flight plan was designed to image each study plot at nadir. The plots were marked in the field using bright ground control points easily detectable on the imagery. The bandsets selected for this study comprised centre wavelengths at 670 and 800 nm with 10 nm full width at half maximum (FWHM) used for computing the NDVI and bands centered at 490, 530, 570 and 700 nm to compute other spectral indices such as the photochemical reflectance index (PRI) for stress detection studies, and the red edge for chlorophyll estimation.

Diurnal campaigns were conducted for both airborne imagery acquisition and intercepted PAR field measurements collected every hour from 8.00 to 12.00 GMT (8.00–12.00 GMT on citrus in 2007; 8.00–11.00 GMT on peach in 2008; 10.00 and 12.00 GMT on peach in 2007), thus a total of 11 airborne images were acquired over the selected plots for each orchard. The objective was to study the diurnal variation of the intercepted radiation over the course of the day as a function of the sun geometry. Additionally, to assess the effects of the variability of the intercepted solar radiation and reflectance bands as a function of orchard architecture, a total of 30 additional airborne images were collected over the study plots. Atmospheric correction and radiometric calibration methods were applied to the imagery to calculate the spectral reflectance. Radiometric calibration was conducted in the laboratory using coefficients derived from measurements made with a uniform calibration body (integrating sphere, CSTM-USS-2000C Uniform Source System, LabSphere, NH, USA) at four levels of illumination and eleven integration times. Radiance values were converted to reflectance using the total incoming irradiance simulated with SMARTS (Gueymard 2005) using aerosol optical depth (AOD) at 550 nm measured with Micro-Tops II sunphotometer (Solar LIGHT Co., Philadelphia, PA, USA) collected in the study areas at the time of the imagery acquisition. This radiative transfer model has been previously used in other studies such as Berni et al. (2009) and Suárez et al. (2010). The algorithms used by SMARTS were developed to match the output from the MODTRAN complex band models within 2 %, but uses AOD (aerial optical depth) as input. The geometric calibration was conducted using Bouguet's calibration method (Bouguet 2001) in order to recover the intrinsic camera parameters (Berni et al. 2009).

3D simulation of row-structured tree canopies

A detailed simulation of the land surface bidirectional reflectance was undertaken in order to understand the relationships between canopy architecture and the intercepted PAR as a function of the vegetation canopy structure, tree spatial distribution, and leaf and background optical properties. A 3D model of light interaction with vegetation canopies (FLIGHT) was used for this study. FLIGHT was selected because it allowed simulation of row orientations, tree dimensions, soil background effects, and to generate 3D scenes to assess the effects of the architecture, crown structure and biochemical inputs. The FLIGHT model is based on the Monte Carlo ray tracing method as a tool to simulate the radiative transfer in a canopy structure (North 1996). Monte Carlo simulation allows highly accurate estimation of light interception and bidirectional reflectance (Barton and North 2001; Disney et al. 2000). The technique requires sampling of the photon free-path within a canopy representation, and simulation of the scattering event at each iteration. An accurate treatment of light interception and multiple scattering between foliage elements and the soil boundary is obtained by iteration (North 2002). In addition to calculating absorbed or intercepted radiation, the model also allows direct calculation of canopy photosynthesis,

Author's personal copy

accounting for structure and anisotropic down-welling radiation field (Alton et al. 2007). The FLIGHT model has been assessed with other three-dimensional codes as part of the radiation model intercomparison (RAMI) project (Widlowski et al. 2007). The recent analysis within RAMI of six selected three-dimensional models, including FLIGHT, showed dispersion within 1 % over a large range of canopy descriptions (Widlowski et al. 2008).

Canopy model assessment for simulating row tree orchards

The FLIGHT model inputs consisted of: (i) geometric characteristics: crown shape, height, and radius, leaf angle distribution, LAI and location of each single crown in the scene, as well as trunk geometry, total scene size and vegetation coverage; (ii) optical properties: soil reflectance and green leaf reflectance and transmittance; (iii) sun and view azimuth and zenith angles; and (iv) other parameters such as soil roughness, aerosol optical thickness and the number of photons simulated. Table 1 shows the input parameters required to run the FLIGHT model for the scenes simulated in this study. The output of the model simulation is a 3D hyperspectral image with the same number of bands as the input leaf spectral signature and the estimated intercepted PAR (IPAR) for the scene.

A detailed simulation of the canopy reflectance was undertaken to assess the performance of the FLIGHT model for this type of row-tree structure canopy. Table 2 shows the selected plots used for the 3D canopy model assessment. The study areas were selected to assure spatial variability, showing a wide range in vegetation cover fraction: 9–60 % in peach, and 4–75 % in citrus orchards, as well as different row orientations (N–S; E–W) and tree heights (1.8–4 m). In addition, flights conducted at different times enabled the assessment of the diurnal evolution of canopy reflectance and fIPAR estimated by the 3D model. FLIGHT simulations were conducted with structural and optical measurements collected at each plot (see Fig. 4 for the optical properties and Table 2 for the structural parameters used). Model assessment for the canopy reflectance simulations was conducted by comparisons between the modeled reflectance and the airborne imagery reflectance acquired on each plot and flight time, calculating the RMSE.

Assumptions considered in the modeling work consisted of fixed leaf angle distribution for all trees on the scene. In addition, the trees in a 3D scene had the same shape, which corresponded to the mean value measured for the four central trees on each site. The woody material (NPV) was not considered as field measurements conducted indicated less than 8 % NPV, and negligible effects were found on the reflectance and NDVI values used to relate with fIPAR. Fruits for peach trees were not considered in the simulations.

Scaling up and model inversion methods for fIPAR estimation

The FLIGHT model was tested to assess the accuracy of the simulations for fIPAR in row-structured tree canopy scenes. To assess the influence of the architecture on the canopy reflectance on the aggregated NDVI and on fIPAR, the FLIGHT input parameters were varied and the simulated reflectance per plot was aggregated by the four central trees of the plot, including the soil between tree rows and shadows (see Fig. 1a, b). *Scaling-up* and model inversion methods were conducted to estimate the instantaneous fIPAR in the row-tree orchards using the airborne imagery acquired on each study site.

For the *scaling-up* method, the objective was to develop predictive relationships NDVI–fIPAR calculated under specific canopy assumptions. The predictive relationships for the peach and citrus orchards were obtained with input parameters fixed according to mean field measurements for each orchard: leaf angle distribution function, leaf optical

Author's personal copy

Table 3 Variables used to generate predictive relationships and LUT for the *scaling-up* and model inversion methods

	Scaling-up	Model inversion (LUT)
Fixed parameters		
Leaf (ρ and τ)	See Fig. 4	See Fig. 4
LADF	See Fig. 5	See Fig. 5
Row orientation	NS (peach) EW (orange)	NS (peach) EW (orange)
Sun geometry	SZ: 35.02°; SA: 69.5° (peach) SZ: 47°; SA: 49.2° (orange)	SZ: 35.02°; SA: 69.5° (peach) SZ: 47°; SA: 49.2° (orange)
Soil (ρ_s)	Extracted from image	–
Variable parameters		
Tree radius (m)	0.5–2	0.5–2
Tree height (m)	1.4–5	1.4–5
LAI	2–6	2–6
Soil (ρ_s)	–	See Fig. 10
Results	r^2; (RMSE)	r^2; (RMSE)
NDVI		
Peach	0.87; (0.08)	0.84; (0.12)
Citrus	0.88; (0.09)	0.85; (0.08)
Four bands (570, 670, 700 800 nm)		
Peach	–	0.82; (0.11).
Citrus		0.76; (0.08)

Coefficients of determination and RMSE values obtained between the ground-measured fIPAR and the estimated fIPAR by *scaling-up* and model inversion for both peach and citrus orchards

SZ solar zenith (degrees from the vertical), *SA* solar azimuth (degrees from South, clockwise negative)

properties, row orientation and soil reflectance extracted from the airborne image, and the solar geometry depending on the time of flight. The methods used in this study are relevant for fully dressed peach trees and for the entire season in perennial citrus orchards. A specific set of input parameters for the FLIGHT model typical for these orchards to define the canopy structure were: 0.5–2 m in the case of crown radii, tree height ranged from 1.4 to 4 m, and LAI from 2 to 6. Table 3 shows a summary of all input parameters used for the *scaling-up* method. The modeled relationships NDVI versus fIPAR obtained for each orchard were then applied to the multi-spectral airborne imagery reflectance to estimate the instantaneous fIPAR for each flight time and study site. This methodology enabled the application of sensor-derived optical indices for scaled-up relationships NDVI–fIPAR that are a function of canopy structure, optical properties and the viewing geometry.

The estimation of fIPAR based on model inversion was conducted by using *look-up* tables (LUT) developed independently for each orchard type, using the specific leaf spectral properties, row orientation and sun geometry. The range of parameters used to define the canopy structure was the same as in the *scaling-up* methodology, while including the variability in the soil optical properties (Table 3). A total of 1 000 synthetic spectra were generated using the FLIGHT model with random input parameters within the ranges previously proposed. The 1 000 synthetic spectra were composed of 9 bands with

Author's personal copy

wavelength centres at 400, 450, 500, 570, 600, 670, 700, 750 and 800 nm to simulate the bands acquired by the airborne sensor. The FLIGHT model used for fIPAR estimation was first tested with synthetic spectra using a numerical model inversion method. A subset of 500 synthetic spectra was used to build the LUT, and the remaining subset used for model inversion to assess the retrieval of fIPAR. This step was conducted to assess the robustness of the FLIGHT model for retrieving fIPAR. Next, the reflectance spectra obtained from the imagery for each study site were used as input for the model inversion method to estimate fIPAR for each study area. For this step, the 1 000 synthetic spectra LUT was used, and the error calculation consisted of determining the set of reflectance spectra which minimized the merit function Δ^2, Eq. 5.

$$\Delta^2 = \sum_n [r_m(\lambda_i) - r^*(\lambda_i)]^2 \tag{5}$$

where $r_m(\lambda_i)$ is the canopy spectral reflectance from the LUT; $r^*(\lambda_i)$ is the canopy spectral reflectance inverted. In the present study, two methods were used in the inversion procedure, (i) using reflectance bands centred at wavelength 570, 670, 700 and 800 nm; and (ii) building the merit function based on the NDVI index. This methodology has been previously applied by Weiss et al. (2000) and Koetz et al. (2005) for LAI estimation.

Results and discussion

Using the FLIGHT model for row-structured tree canopies: canopy reflectance assessment

A sample FLIGHT simulation scene corresponding to the orange orchard at different sun angles is shown in Fig. 7a. Block spectra (Fig. 1) were extracted from the airborne imagery and simulation scenes, and vegetation indices calculated. Reflectance spectra comparisons were made between model simulations and airborne imagery, assessing the canopy reflectance simulations for the VIS and NIR wavelengths. Figure 7 shows image-extracted and simulated canopy reflectance for the peach orchard (Fig. 7b) and orange orchard (Fig. 7c) at different times. Leaf optical properties and LADF data appear in Figs. 4 and 5. The image data used in this study were collected in 2 years. The multi-spectral sensor has configurable bandsets. Thus, during 2007, the selected wavelengths were 530, 570, 670, 715, 730 and 800 nm and, in 2008, the bands used were 530, 550, 570, 670, 700 and 800 nm. Both datasets had the bands required for NDVI calculation. The trend observed in the airborne imagery as a function of sun angle showed an increasing canopy reflectance with time due to the reduced shadow proportions, which were well captured by the model. This effect is more evident in N–S oriented orchards (Fig. 7b), as the shaded contribution changes more significantly in this orientation than in E–W orientation (Fig. 7c).

The green (570 nm), red (670 nm) and NIR (800 nm) bands extracted from the imagery acquired over the study plots were compared against simulations conducted with the FLIGHT model (Fig. 8a). The FLIGHT input parameters used were measured for each study site (Table 2; Figs. 4, 5). The simulations for the green spectral band (10 nm FWHM) yielded RMSE values of 0.011 and 0.024 for orange and peach, respectively; similar results were obtained for the red band (RMSE = 0.017 and 0.031). For the NIR band, the errors increased slightly (RMSE = 0.05). Higher errors were obtained for N–S orientation as compared to E–W due to higher changes in reflectance over the diurnal

Author's personal copy

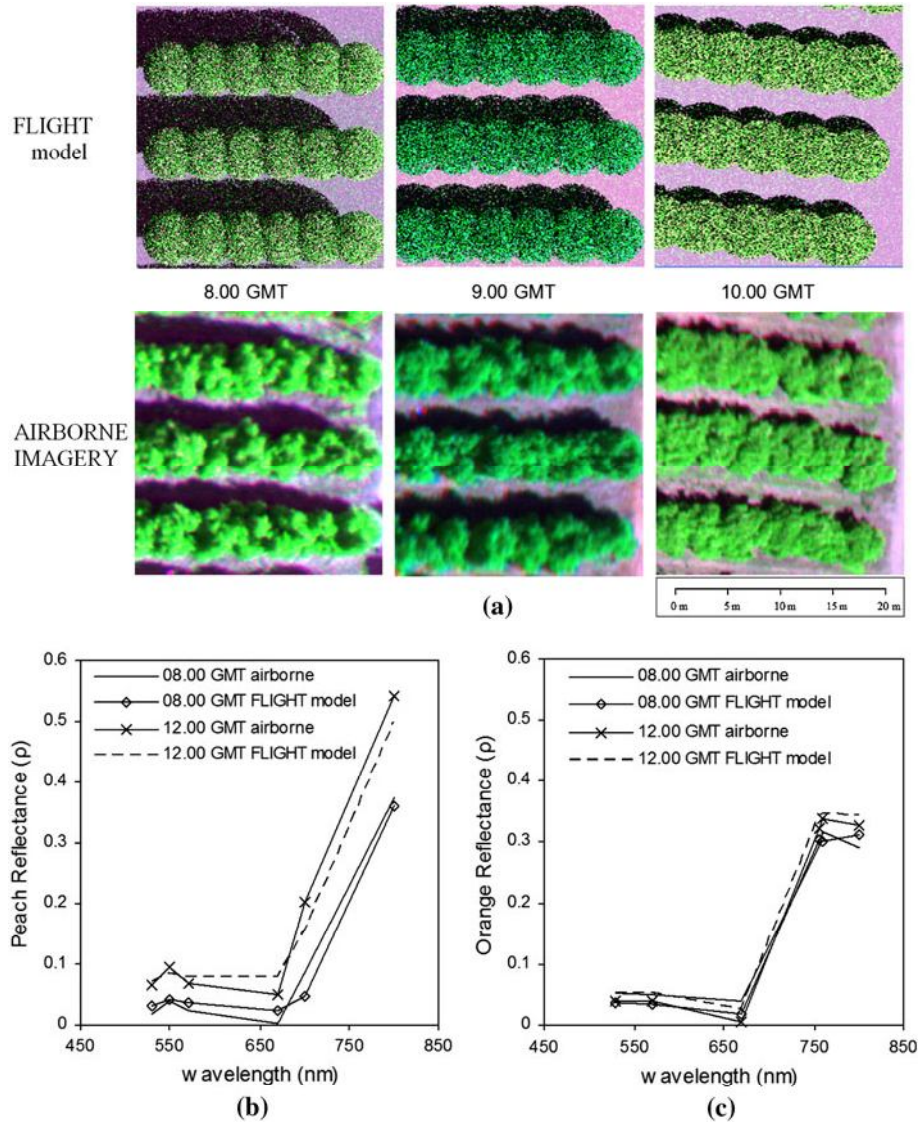

Fig. 7 UAV airborne imagery acquired from one study site, and the corresponding simulations conducted with FLIGHT at 8.00, 9.00 and 10.00 GMT (**a**). Spectra obtained for aggregated vegetation-soil pixels: multi-spectral image spectra collected at 8.00 and 12.00 GMT, and canopy simulations conducted with FLIGHT on peach (**b**) and orange (**c**) orchards

course. The RMSE values obtained for all bands in the VIS were below 0.03, and below 0.05 in the NIR.

Assessments conducted for NDVI and fIPAR simulated with FLIGHT and obtained from the airborne imagery (NDVI) and ceptometer (fIPAR) are shown in Fig. 8b and c, respectively. The analysis of NDVI yielded RMSE = 0.06–0.07 in orange and peach orchards, respectively, obtaining RMSE values of 0.06 (peach) and 0.08 (orange) for fIPAR. Plots with low vegetation cover fraction presented higher errors in the simulations

Author's personal copy

Fig. 8 Relationships obtained for canopy reflectance at 570, 670 and 800 nm (**a**), NDVI (**b**), and fIPAR (**c**) calculated from multi-spectral airborne imagery and FLIGHT simulations

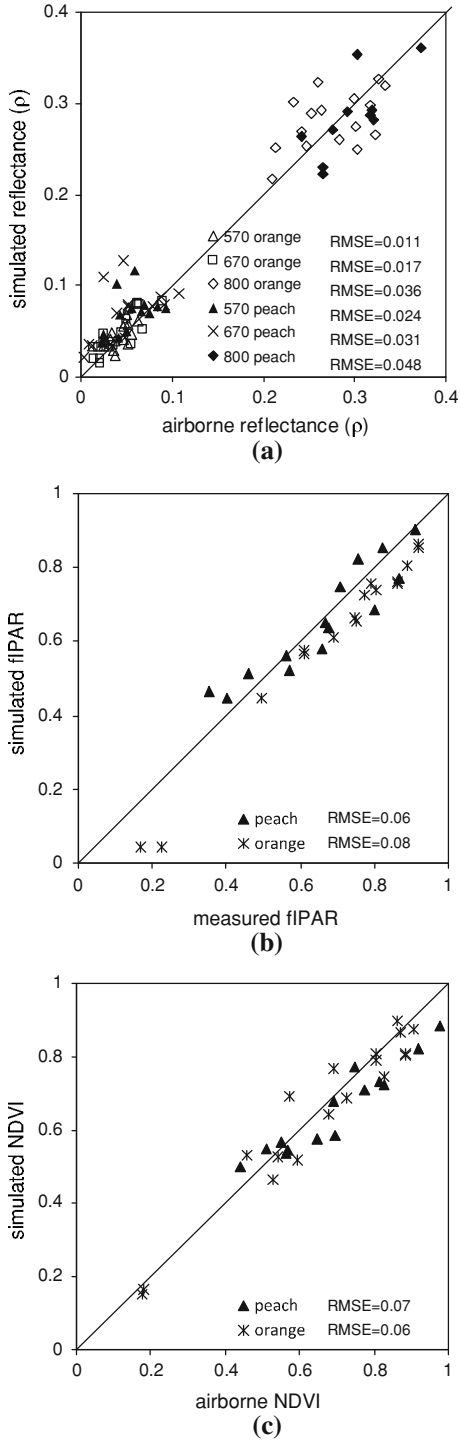

Author's personal copy

conducted for fIPAR estimation. Considering the complex canopy architecture simulated, the large number of field measurements required for simulations and the atmospheric and image calibration issues, these results seemed acceptable for simulating the 3D row structure architecture conducted with FLIGHT.

Simulation results for fIPAR in row-structured tree canopies

Simulations with FLIGHT were conducted to understand the sensitivity of input parameters, such as vegetation cover fraction, sun angles, row orientation, LAI and the soil reflectance, on the canopy reflectance (ρ), NDVI and fIPAR simulations. The red (670 nm) and NIR (800 nm) bands used for NDVI calculation and fIPAR were simulated as a function of the sun angle for N–S and E–W row orientations for a range of vegetation cover fraction (30–70 %) and soil spectra (bright, medium and dark). The effects of the row orientation on NDVI and fIPAR were studied by generating different canopy scenarios on a summer day as shown in Fig. 9. The figure illustrated three scenarios: NS row oriented tress (Fig. 9a), EW row oriented trees (Fig. 9b) and randomly distributed trees (Fig. 9c) at 10.00 GMT. All three cases had the same cover vegetation fraction, but variable percentage shadow due to the tree spatial distribution. The vegetation cover fraction was 48 % and LAI = 4 in all cases, the height of the trees was set to 2.7 m, and a spherical leaf angle distribution function was assumed. This figure highlights the importance of considering row orientation in the simulations. As such, the analysis focused on row-orientated orchards, while excluding the random distribution simulations. The effects of the background were assessed because it is well accepted that variations in soil spectral reflectance have significant effects on NDVI (Huete et al. 1985), especially in open canopies. In our analysis, three different types of soil reflectance were considered, representing dark, medium and bright soils (Fig. 10). For N–S row orientations (Fig. 11a, d, g), larger differences on ρ, NDVI and fIPAR were found as a function of sun angles. NIR and red bands increased up to 0.20 for bright soils from morning until midday,

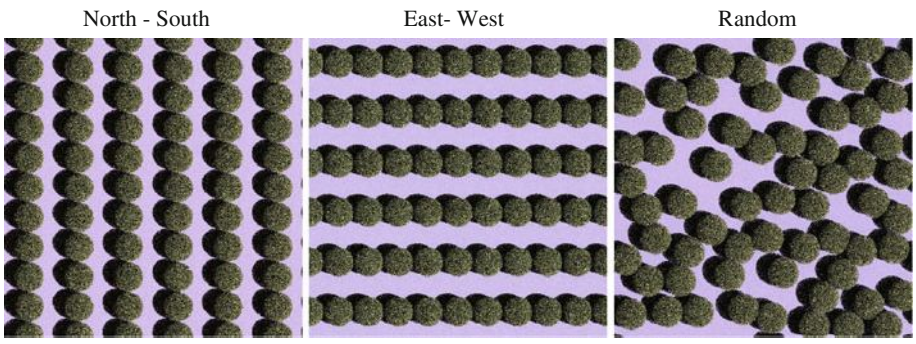

Time 10.00 GMT: *SZ*: 35.02º; *SA*: 69.47º

SZ: Solar zenith (degrees from North)

SA: Solar azimuth (degrees from South, clockwise negative)

Fig. 9 FLIGHT model simulations generating orchard scenes for two different row orientations, NS and EW (**a** and **b** respectively) and a random distribution (**c**). Input parameters were: LAI = 4, fractional cover = 0.48, leaf size = 0.025, fraction of green leaves = 0.85, fraction of bark = 0, ladf = spherical, crown shape = ellipsoidal, crown radius = 1.5 m, tree height = 2.7 m, soil roughness = 0, aerosol optical thickness = 0.1

Author's personal copy

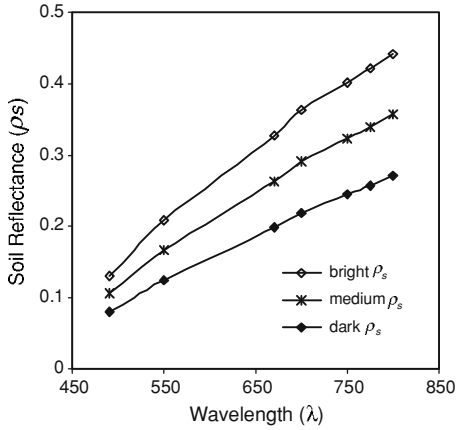

Fig. 10 Spectral reflectance for three different soil brightness levels

while the diurnal variation of ρ on scenes with dark soils was around 0.10. These differences found between ρ at morning and noon appeared slightly smaller for greater ground cover (70 %) (Fig. 11a). For NDVI, a decrease of up to 0.4 was shown for a dark soil background from 8.00 to 12.00 GMT. Soil spectra had significant influence on NDVI, mainly at midday (Fig. 11d). The trend for fIPAR was similar to NDVI, decreasing between 0.3 and 0.4 for both canopy cover values, but with little effect caused by the background (Fig. 11g). On the contrary, simulations conducted demonstrated the small sun angle effect on ρ, NDVI and fIPAR for E–W orientations (Fig. 11b, e, h). As expected, row-tree lines oriented in the solar plane made the shaded soil component variation a very small contribution to the canopy reflectance (Fig. 11b, e), and on fIPAR (Fig. 11h). However, large differences on canopy reflectance, NDVI and fIPAR were found when the vegetation cover fraction was varied, as expected. Changes in soil reflectance affected the canopy reflectance simulations and NDVI (Fig. 11b, e), while fIPAR simulation was less affected by the background (Fig. 11h). Variations in the LADF had small effects (Fig. 11c, f, i). These results demonstrate the importance of canopy modeling methods to understand the behaviour of reflectance, NDVI and fIPAR for different canopy scenarios on row-structured canopies.

The instantaneous NDVI–fIPAR relationships as a function of fixed and variable inputs were calculated to build *scaling-up* relationships. The sun geometry was fixed to 10.00 GMT for a summer day (zenith = 35.02° from North; azimuth = 69.47° from South, clockwise negative) and variation was driven by the vegetation cover fraction (4–70 %). The architectural canopy parameters such as tree height (z) were varied for three different levels (z = 1.7; 2.9; 4 m) showing a marginal effect on the NDVI–fIPAR relationship (Fig. 12a). Similar results were found for the LAI variation (data not shown), which confirms previous studies, such as Goward and Huemmrich (1992). The instantaneous NDVI–fIPAR relationships for N–S and E–W row orientations, in combination with changes in the soil optical properties, were also studied for two different sun angles: morning (8.00 GMT) (Fig. 12b) and midday (12.00 GMT) (Fig. 12c). At 8.00 GMT, soil reflectance had a significant effect on the NDVI–fIPAR relationship for the E–W row orientation (Fig. 12b), being less important for N–S row orientation because the soil is completely shaded at such a sun angle (8.00 GMT). On the other hand, shadows almost disappeared at 12.00 GMT. Soil optical properties caused large effects on both E–W and N–S orientations (Fig. 12c). For example, for NDVI = 0.4, differences of 0.17 in fIPAR were found as a function of bright and dark soils (Fig. 12c) for both orientations. The canopy model results showed high sensitivity of the NDVI–fIPAR relationships to the soil optical properties and row orientation, dependant on the sun geometry.

Author's personal copy

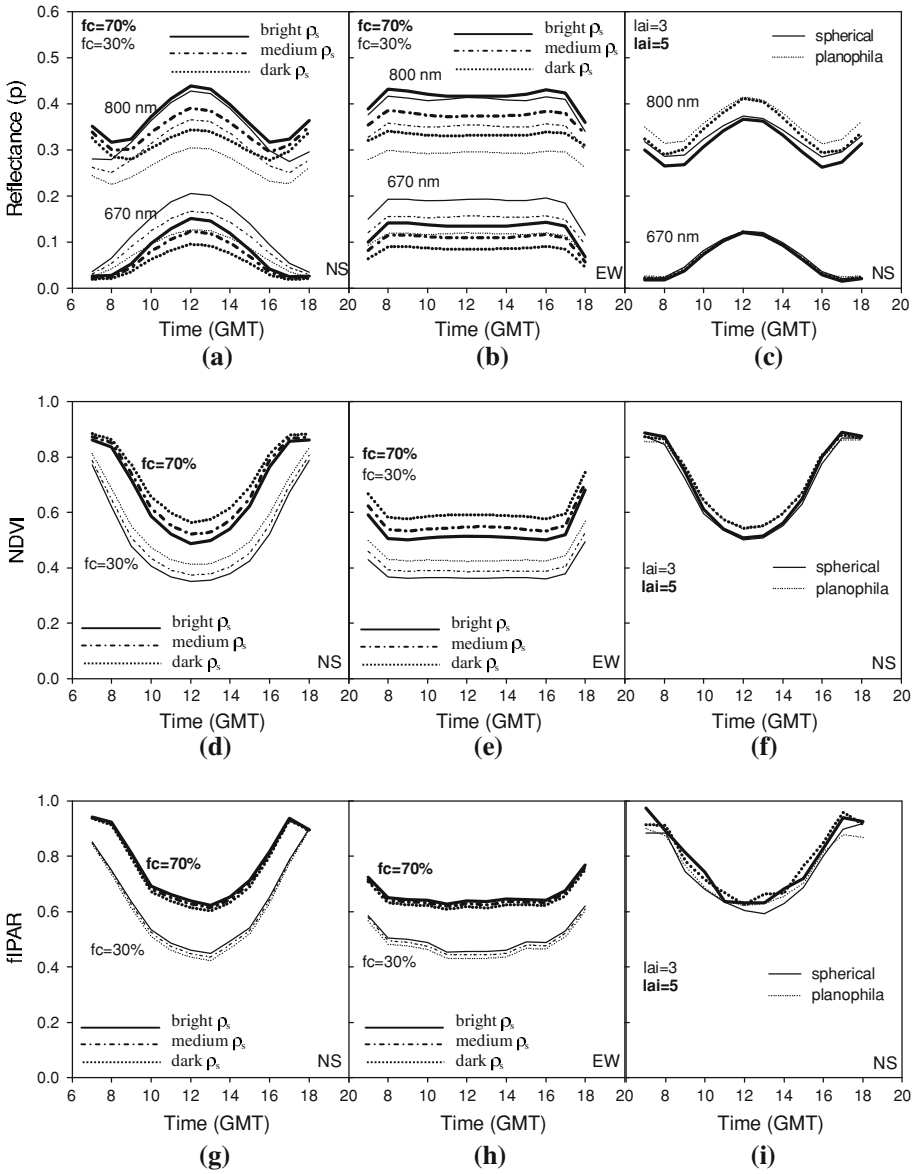

Fig. 11 Simulations obtained with FLIGHT: variance analysis due to effect of the sun geometry on reflectance (670 and 800 nm), NDVI and fIPAR, considering row orientation N–S (**a**, **d**, **g**) and E−W (**b**, **e**, **h**) as a function of different soil background and vegetation cover fraction (30 and 70 %) for LAI = 4 and ladf = spherical. Effects of sun geometry on reflectance (670 and 800 nm), NDVI and fIPAR, considering row orientation N–S as function of different ladf (spherical and planophile) and LAI (3 and 5), medium brightness soil reflectance and 70 % vegetation cover fraction (**c**, **f**, **i**)

Estimating intercepted radiation by scaling up and model inversion methods

An analysis of fIPAR estimation with remote sensing imagery was first conducted by obtaining relationships between vegetation indices calculated from the airborne imagery

Author's personal copy

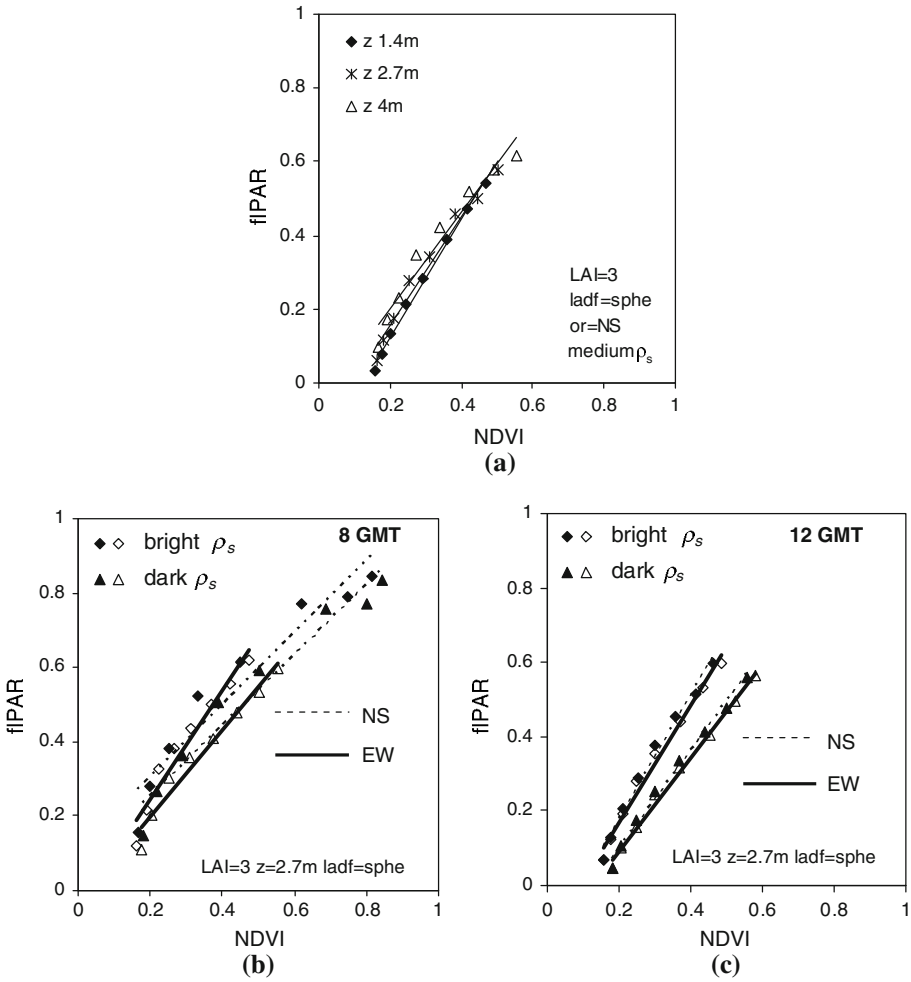

Fig. 12 Variance in the NDVI–fIPAR relationship as a function of tree height (**a**), soil type and row orientation for 8.00 GMT (**b**) and 12 GMT (**c**)

and fIPAR measured with a ceptometer (Fig. 13). The aggregated image reflectance from the four central trees of the orchard, including exposed soil and shadows, was used to compute SVI, such as NDVI. The diurnal variation of NDVI for the same plot over the course of the day as related to fIPAR (Fig. 13a) was mainly driven by soil and shadow variation as a function of the sun geometry. The spatial variation of NDVI versus fIPAR (Fig. 13b) was obtained through measurements conducted at selected plots with different architectural canopy characteristics at 10.00 GMT (±half hour). The results showed high coefficients of determination for NDVI versus fIPAR with $r^2 > 0.9$ for the diurnal trial, and $r^2 > 0.8$ for the spatial variation study. Methodologies to estimate instantaneous fIPAR through *scaling-up* and model inversion methods were then investigated.

Modeled relationships NDVI versus fIPAR were obtained by the *scaling-up* methodology (Fig. 14a). Parameters used to obtain these relationships can be found in Table 3. After previous understanding of the influence of different parameters on the relationship

Author's personal copy

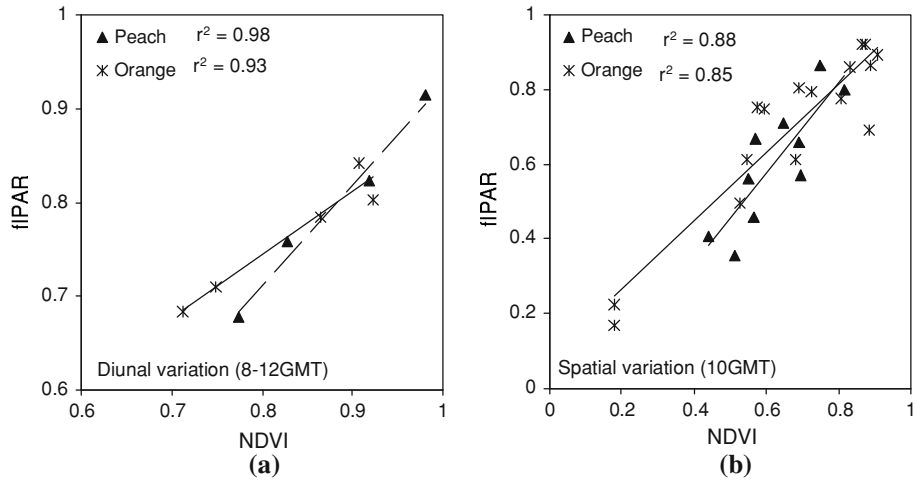

Fig. 13 Relationships obtained between NDVI, calculated from high-resolution airborne imagery, and field-measured fIPAR at different sun angles (diurnal variation) for **a** an individual site and, **b** multiple sites imaged at solar zenith angle = 35° (spatial variation)

NDVI–fIPAR, parameters known for each study area were used, such as row orientation, soil reflectance obtained from the airborne imagery and sun geometry function of the time of each flight. Other canopy architecture parameters were varied within a range (Table 3). Estimation of fIPAR by scaling-up was compared against ground-measured fIPAR for each plot. Relationships obtained for the citrus orchard yielded estimates with relative RMSE of 0.10 and $r^2 = 0.88$. For the peach orchard, a relative RMSE of 0.08 and $r^2 = 0.87$ were obtained (Fig. 14b).

The simulation study to investigate the retrieval of fIPAR through FLIGHT radiative transfer model inversion was conducted by iteration from the synthetic spectra for peach (Fig. 15a) and orange orchards (Fig. 15b). The fIPAR estimates shown in Fig. 15 were obtained using two approaches. In the first case, only four of the nine bands, 570, 670, 700 and 800 nm, were used for the inversion, and the second case using NDVI. In addition, during the model inversion, some parameters were fixed and others were varied (see Table 3) to simulate the typical set of parameters potentially known and unknown. That is the reason for the scatter in the plots between estimated fIPAR and fIPAR calculated from the synthetic spectra. Relative RMSE below 0.09, and coefficients of determination around 0.8 were obtained by using the four bands and NDVI for the model inversion method for both orchards. The modeling exercise conducted with synthetic spectra demonstrated the feasibility of the proposed model inversion method to retrieve fIPAR with the FLIGHT model.

Subsequently, the estimation of fIPAR by inversion using airborne imagery was compared with ground-measured fIPAR for each plot. LUTs were generated as indicated in Table 3. Results obtained from comparing the estimated fIPAR by radiative transfer model inversion against the field-measured fIPAR (Fig. 15c, d) yielded a relative RMSE of 0.08 and 0.10 for orange and peach orchards, respectively. Building the merit function with (i) four bands, and (ii) NDVI, did not show significant differences. Results obtained by comparing the estimated fIPAR against field measurements demonstrated the feasibility of the model inversion approach for fIPAR estimation using the FLIGHT model.

Author's personal copy

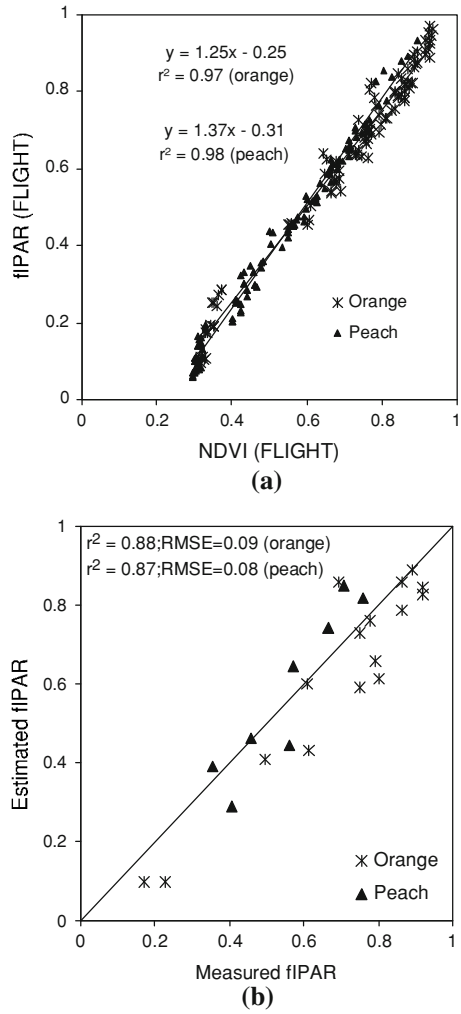

Fig. 14 Relationships between fIPAR and NDVI obtained for FLIGHT for citrus and peach orchards (**a**). Estimated intercepted radiation using *scaling-up* equations developed in **a**, versus measured fIPAR (**b**)

A direct application of these methodologies enabled obtaining maps of the instantaneous intercepted radiation at orchard scale using the airborne imagery. The maps obtained for citrus and peach orchard showing the variation of the vegetation cover fraction, together with the estimated fIPAR are shown in Figs. 16 and 17. Large differences can be observed between the different study areas, with values of intercepted radiation ranging from 0.18 to 0.88.

Conclusions

This work examines the relationship between canopy reflectance and instantaneous fIPAR in peach and citrus orchards using the 3D radiative transfer FLIGHT model and measurements conducted with ground and remote instruments on board an UAV. VIS and NIR canopy reflectance and fIPAR simulations conducted with FLIGHT were assessed for these row-structured canopies, obtaining a RMSE below 0.03 for the VIS bands, and below 0.05

Author's personal copy

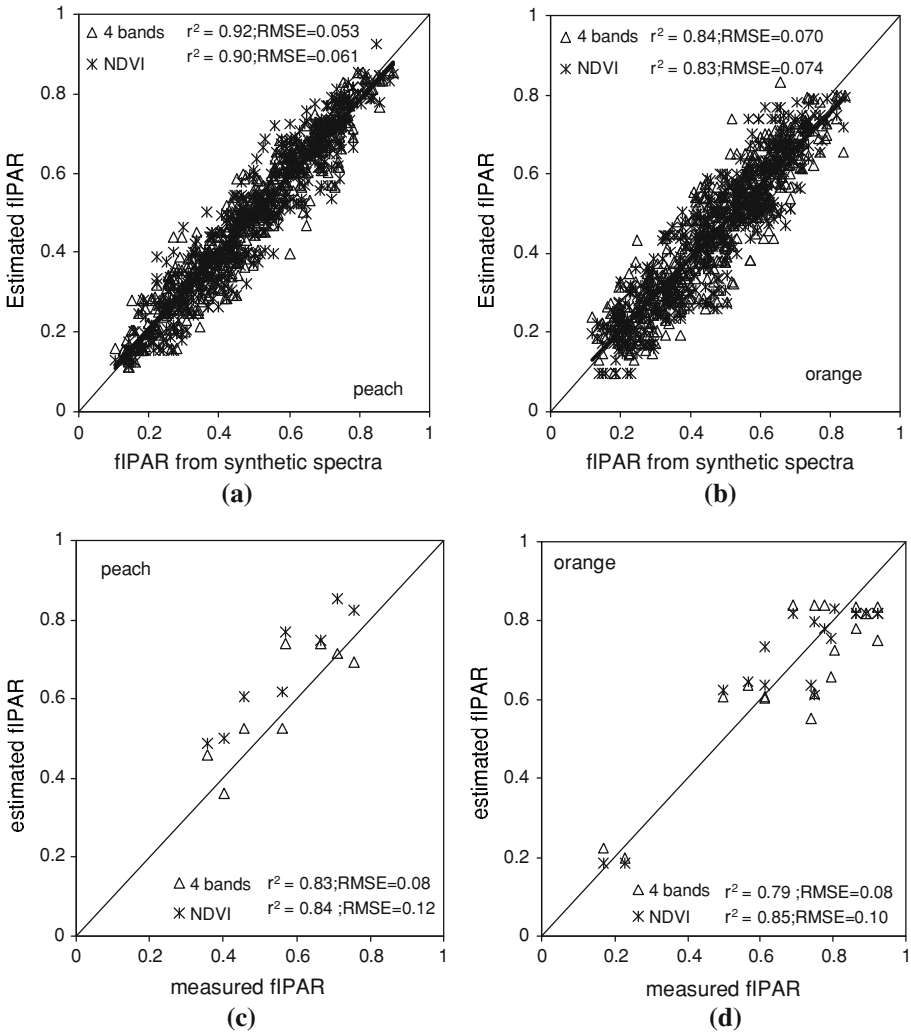

Fig. 15 Coefficients of determination and RMSE obtained between fIPAR obtained from synthetic spectra for peach (**a**) and citrus orchards (**b**). Coefficient of determination and RMSE obtained between field-measured fIPAR and estimated fIPAR by inversion for peach (**c**) and citrus orchards (**d**)

for the NIR band. The main drivers of the relationship NDVI–fIPAR in these heterogeneous canopies were the background optical properties and the row orientation, both as a function of the sun geometry. The background reflectance had significant effects on the aggregated NDVI at midday, when the proportion of shaded soil is minimal. As a consequence, the NDVI–fIPAR relationships were independent of the row orientation at noon. It was demonstrated that the NDVI–fIPAR relationship changes as a function of the soil optical properties and row orientation, due to their large effects on NDVI in non-homogeneous orchard canopies.

This study demonstrated that a robust NDVI–fIPAR relationship can be obtained for row-structured peach and citrus orchards using 3D simulations when accounting for the

Author's personal copy

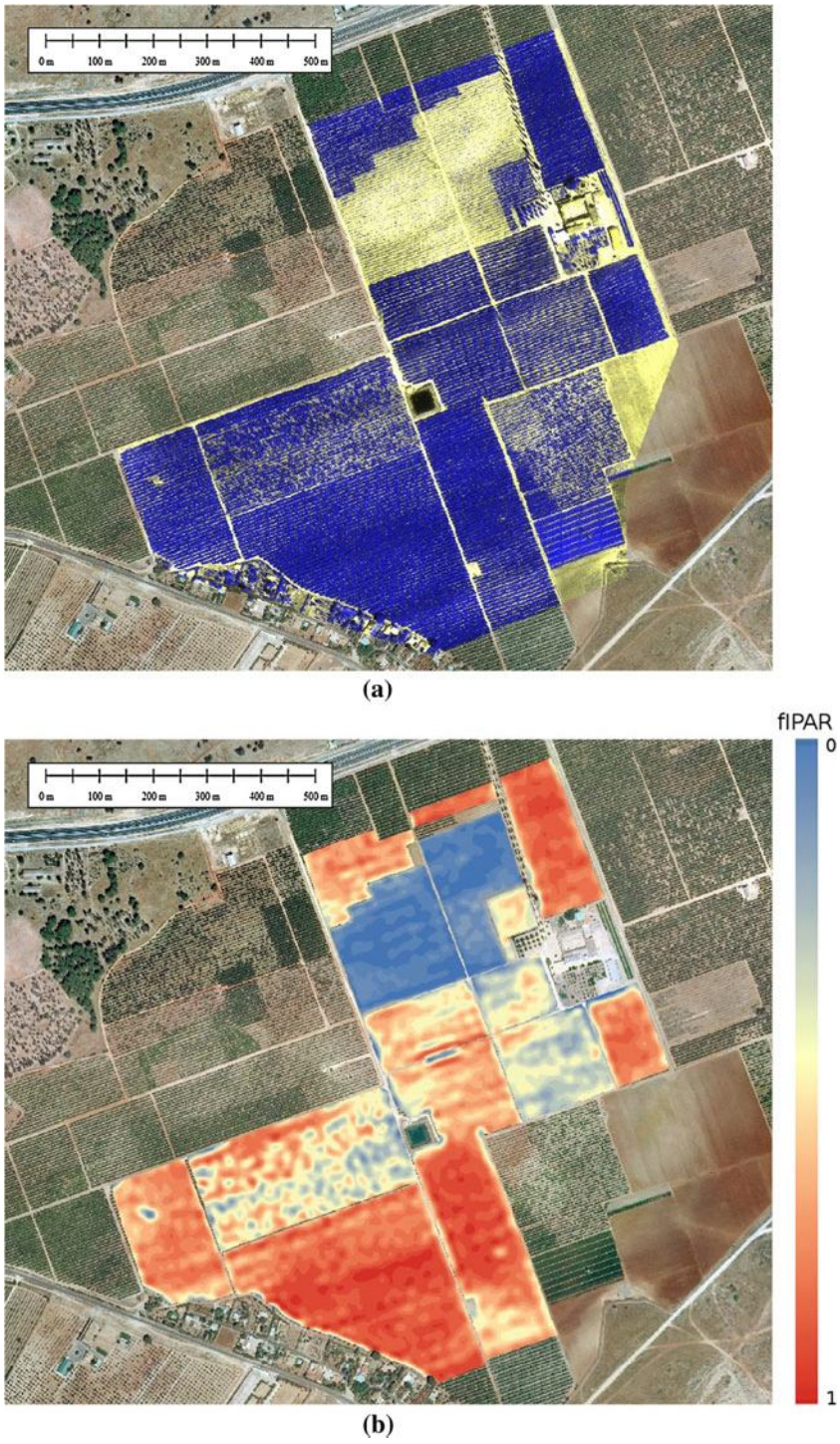

Fig. 16 Multi-spectral mosaic of the citrus orchard acquired from the UAV platform (**a**) used to generate a map of fIPAR calculated from the FLIGHT model (**b**)

Author's personal copy

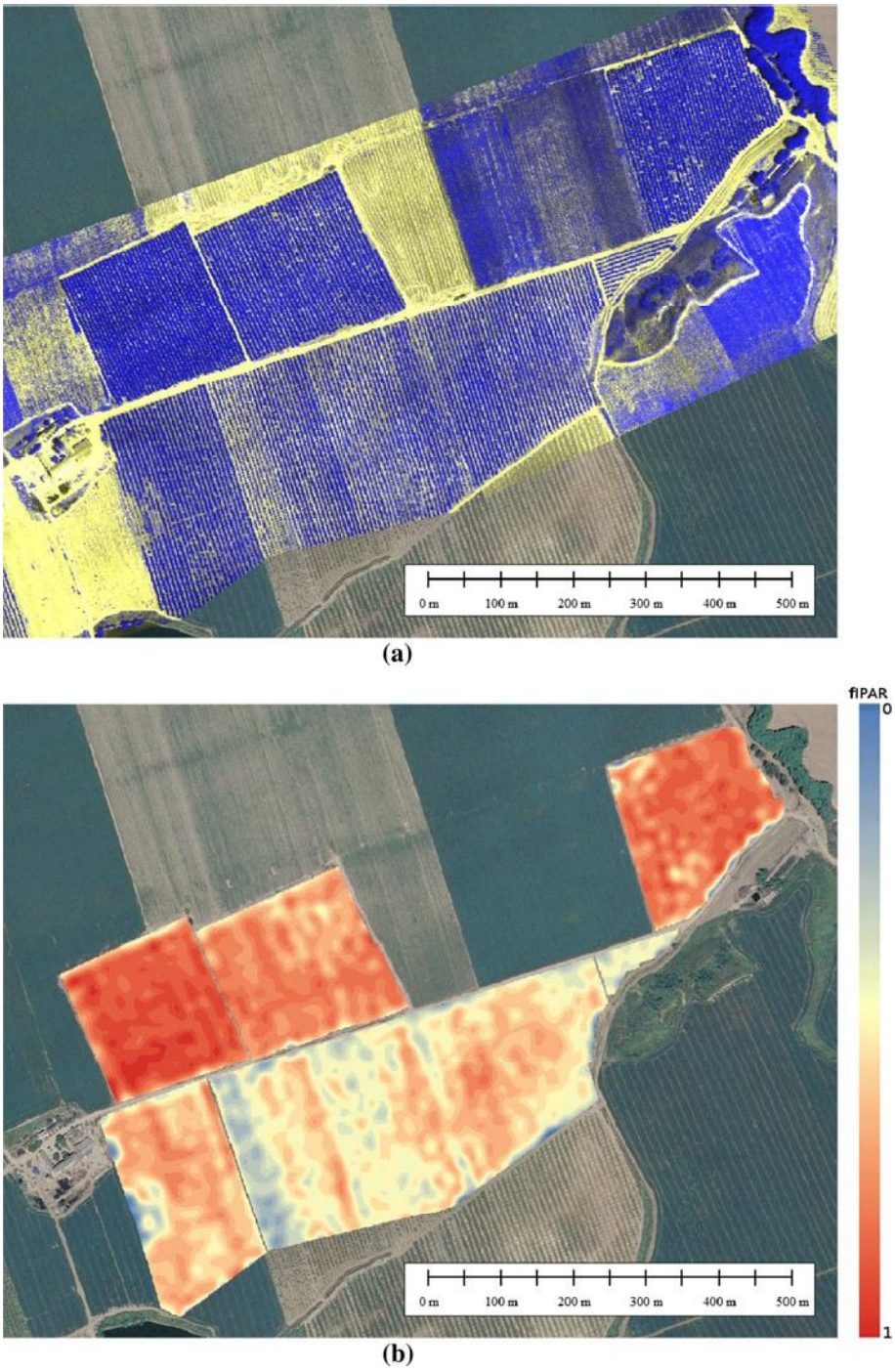

Fig. 17 Multi-spectral mosaic of the peach orchard acquired from the UAV platform (**a**) used to generate a map of fIPAR calculated from the FLIGHT model (**b**)

Author's personal copy

soil optical properties, sun angles and row orientation. The proposed methods, based on *scaling-up* and model inversion techniques, may be applied to NDVI pixels acquired over heterogeneous orchards to obtain maps of instantaneous intercepted radiation. The methodology demonstrates the feasibility for estimating the spatial distribution of fIPAR in citrus and peach row-structured orchards, yielding RMSE below 0.10. The generation of high-resolution maps of the intercepted radiation using multi-spectral cameras mounted on operational UAV platforms may be of critical interest for precision agriculture tasks such as the agronomic management of homogeneous zones and the discrimination of potential fruit quality areas for harvest.

Acknowledgments Financial support from the Spanish Ministry of Science and Innovation (MCI) for the projects AGL2009-13105, CONSOLIDER CSD2006-67, and AGL2003-01468 is gratefully acknowledged, as well as the Junta de Andalucía-Excelencia AGR-595 and FEDER. M.L. Guillén-Climent was supported by a grant JAE of CSIC, co-funded by the *European Social Fund*. Technical support from UAV Navigation, Tetracam Inc. and UAV Services and Systems for the airborne requirements are acknowledged. A. Vera, D. Notario, R. Romero, and A. Hornero are acknowledged for technical support in field and airborne campaigns.

References

Alton, P. B., North, P. R., & Los, S. O. (2007). The impact of diffuse sunlight on canopy light-use efficiency, gross photosynthetic product and net ecosystem exchange in three forest biomes. *Global Change Biology, 13*, 1–12.

Asrar, G., Myneni, R. B., & Choudbhury, B. J. (1992). Spatial heterogeneity in vegetation canopies and remote sensing of absorbed photosynthetically active radiation: A modelling study. *Remote Sensing of Environment, 41*, 85–103.

Barton, C. V. M., & North, P. R. J. (2001). Remote sensing of canopy light use efficiency using the photochemical reflectance index. Model and sensitivity analysis. *Remote Sensing of Environment, 78*, 264–273.

Berni, J. A. J., Zarco-Tejada, P. J., Suarez, L., & Fereres, E. (2009). Thermal and narrow-band multispectral remote sensing for vegetation monitoring from an unmanned aerial vehicle. *IEEE Transactions on Geoscience and Remote Sensing, 47*(3), 722–738.

Bouguet, J. (2001). Camera calibration toolbox for Matlab. http://www.vision.caltech.edu/bouguetj/calib_doc. Accessed January 2012.

Choudhury, B. J. (1987). Relationships between vegetation indices, radiation absorption, and net photosynthesis evaluated by a sensitivity analysis. *Remote Sensing of Environment, 22*, 209–233.

Daughtry, C. S. T., Gallo, K. P., & Bauer, M. E. (1983). Spectral estimates of solar radiation by corn canopies. *Agronomy Journal, 75*, 527–531.

Daughtry, C. S. T., Gallo, K. P., Goward, S. N., Price, S. D., & Kustas, W. P. (1992). Spectral estimates of absorbed radiation and phytomas production in corn and soybean canopies. *Remote Sensing of Environment, 39*, 141–152.

De Wit, C. T. (1959). Potential photosynthesis of crop surfaces, Netherlands. *The Journal of Agricultural Science, 7*, 141–149.

Disney, M. I., Lewis, P., & North, P. R. J. (2000). Monte Carlo ray tracing in optical canopy reflectance modelling. *Remote Sensing Reviews, 18*(2–4), 163–196.

Gallagher, J. N., & Biscoe, P. V. (1978). Radiation absorption, growth and yield of cereals. *The Journal of Agricultural Science, 91*, 47–60.

Goward, S. N., & Huemmrich, K. F. (1992). Vegetation canopy PAR Absorptance and the normalized difference vegetation index: An assessment using the SAIL model. *Remote Sensing of Environment, 39*, 119–140.

Gueymard, C.A. (2005). SMARTS Code, Version 2.9.5 user's manual solar consulting services. Online PDF document from http://www.nrel.gov/rredc/smarts/. Accessed January 2012.

Hall, F. G., Huemmrich, K. F., Goetz, S. J., Sellers, P. J., & Nickerson, J. E. (1992). Satellite remote sensing of surface energy balance: Success, failures, and unresolved issues in FIFE. *Journal of Geophysical Results, 97*, 19061–19089.

Author's personal copy

Huemmrich, K. F. (2001). The GeoSail model: A simple addition to the SAIL model to describe discontinuous canopy reflectance. *Remote Sensing of Environment, 75*, 423–431.

Huemmrich, K. F., & Goward, S. N. (1997). Vegetation canopy PAR Absorptance and NDVI: An assessment for ten species with SAIL model. *Remote Sensing of Environment, 61*, 254–269.

Huete, A. R. (1989). Soil influences in remotely sensed vegetation canopy-spectra. In G. Asrar (Ed.), *Theory-applications of optical remote sensing* (pp. 107–141). New York: Willey.

Huete, A. R., Jackson, R. D., & Post, D. F. (1985). Spectral response of a plant canopy with different soil backgrounds. *Remote Sensing of Environment, 17*, 37–53.

Hunt, R. E. (1994). Relationship between woody biomass & PAR conversion efficiency for estimating net primary production from NDVI. *International Journal Remote Sensing, 15*, 1725–1730.

Jackson, J. E. (1980). Light interception and utilization by orchard systems. *Horticultural Reviews, 2*, 208–267.

Kempeneers, P., Zarco-Tejada, P. J., North, P. R. J., De Backer, S., Delalieux, S., Sepulcre-Cantó, G., et al. (2008). Model inversion for chlorophyll estimation in open canopies from hyperspectral imagery. *International Journal of Remote Sensing, 29*(17–18), 5093–5111.

Koetz, B., Baret, F., Poilvé, H., & Hill, J. (2005). Use of coupled canopy structure dynamic and radiative transfer models to estimate biophysical canopy characteristics. *Remote Sensing of Environment, 95*(1), 115–124.

Lang, A. R. G. (1987). Simplified estimate of leaf area index from transmittance of the sun's beam. *Agricultural and Forest Meteorology, 41*, 179–186.

Lang, A. R. G., Xiang, Y., & Norman, J. M. (1985). Crop structure and the penetration of direct sunlight. *Agricultural and Forest Meteorology, 35*, 8–101.

Lemeur, R. (1973). A method for simulating the direct solar radiation regime in sunflower, Jerusalen artichoke, corn and soybean canopies using actual stand structure data. *Agricultural and Forest Meteorology, 12*, 229–247.

Li-Cor Inc. (1984). Li-Cor model 1800-12 integrating sphere instruction manual (Revision 1984). Li-Cor Incorporated, Lincoln, NE, Publication No. 8305-0034.

Loomis, R. S., & Williams, W. A. (1963). Maximum crop productivity: An estimate. *Crop Science, 3*, 67–72.

Mariscal, M. J., Orgaz, F., & Villalobos, F. J. (2000). Modelling and measurement of radiation interception by olive canopies. *Agricultural and Forest Meteorology, 100*, 183–197.

Monteith, J. L. (1972). Solar radiation and productivity in tropical ecosystems. *Journal of Applied Ecology, 9*, 747–766.

Moran, M. S., Inoue, Y., & Barmes, E. M. (1997). Opportunities and limitations for image-based remote sensing in precision crop management. *Remote Sensing of Environment, 61*(3), 319–346.

Moriondo, M., Maselli, F., & Bindi, M. (2007). A simple model of regional wheat yield based on NDVI data. *European Journal of Agronomy, 26*, 266–274.

Myneni, R. B., & Williams, D. L. (1994). On the relationships between FAPAR and NDVI. *Remote Sensing of Environment, 49*, 200–211.

North, P. R. J. (1996). Three-dimensional forest light interaction model using a Monte Carlo method. *IEEE Transactions on Geoscience and Remote Sensing, 34*(4), 946–956.

North, P. R. J. (2002). Estimation of f_{APAR}, LAI, and vegetation fractional cover from ATSR-2 imagery. *Remote Sensing of Environment, 80*, 114–121.

Pinty, B., Widlowski, J. L., Gobron, N., & Verstraete, M. M. (2002). Uniqueness of multi-angular information—Part 1: A surface heterogeneity indicator from MISR. *IEEE Transactions on Geosciences and Remote Sensing, 40*, 1560–1573.

Prieto-Blanco, A., North, P. R. J., Barnsley, M. J., & Fox, N. (2009). Satellite-driven modelling of net primary productivity (NPP): theoretical analysis. *Remote Sensing of Environment, 113*, 137–147.

Robinson, T., & Lakso, A. (1991). Bases of yield and production efficiency in apple orchard system. *Journal of the American Society for Horticultural Science, 116*(2), 188–194.

Ross, J. (1981). *The radiation regime and architecture of plant stands*. The Hague: W. Junk.

Suárez, L., Zarco-Tejada, P. J., Berni, J. A. J., González-Dugo, V., & Fereres, E. (2009). Modelling PRI for water stress detection using radiative transfer models. *Remote Sensing of Environment, 113*, 730–744.

Suárez, L., Zarco-Tejada, P. J., González-Dugo, V., Berni, J. A. J., Sagardoy, R., Morales, F., et al. (2010). Detecting water stress effects on fruit quality in orchards with time-series PRI airborne imagery. *Remote Sensing of Environment, 114*, 286–298.

Villalobos, F. J., Orgaz, F., & Mateos, L. (1995). Non-destructive measurement of leaf area in olive (*Olea europaea* L.) trees using a gap inversion method. *Agricultural and Forest Meteorology, 73*, 29–42.

Author's personal copy

Weiss, M., Baret, F., Myneni, R. B., Pragnère, A., & Knyazikhin, Y. (2000). Investigation of a model inversion technique to estimate canopy biophysical variables from spectral and directional reflectance data. *Agronomie, 20*(1), 3–22.

Widlowski, J.-L. (2010). On the bias of instantaneous FAPAR estimates in open-canopy forests. *Agricultural and Forest Meteorology, 150*, 1501–1522.

Widlowski, J.-L., Pinty, B., Disney, M., Gastellu-Etchegorry, J.-P., Lavergne, T., Lewis, P. E., et al. (2008). The RAMI on-line model checker (ROMC): A web-based benchmarking facility for canopy reflectance models. *Remote Sensing of Environment, 112*(3), 1144–1150.

Widlowski, J.-L., Taberner, M., Pinty, B., Bruniquel-Pinel, V., Disney, M., Fernandez, R., et al. (2007). Third radiation transfer model intercomparison (RAMI) exercise: Documenting progress in canopy reflectance models. *Journal of Geophysical Research, 112*, D09111.

Zarco-Tejada, P. J., Berjón, A., López-Lozano, R., Miller, J. R., Martín, P., Cachorro, V., et al. (2005). Assessing vineyard condition with hyperspectral indices: Leaf & canopy reflectance simulation in a row-structured discontinuous canopy. *Remote Sensing of Environment, 99*, 271–287.

Zarco-Tejada, P. J., Berni, J. A. J., Suárez, L., & Fereres, E. (2008). A new era in remote sensing of crops with unmanned robots. *SPIE Newsroom,*. doi:10.1117/2.1200812.1438.

Zarco-Tejada, P. J., González Dugo, V., & Berni, J. A. J. (2012). Fluorescence, temperature and narrow-band indices acquired from a UAV platform for water stress detection using a micro-hyperspectral imager and a thermal camera. *Remote Sensing of Environment, 117*, 322–337.

Zhang, Q., Middleton, E. M., Margolis, H. A., Drolet, G. G., Barr, A. A., & Black, T. A. (2009). Can a satellite-derived estimate of the fraction of PAR absorbed by chlorophyll ($FAPAR_{chl}$) improve predictions of light-use efficiency and ecosystem photosynthesis for a boreal aspen forest? *Remote Sensing of Environment, 113*, 880–888.